

Molecular hydrogen jets and outflows in the Serpens south filamentary cloud

G. D. C. Teixeira¹, M. S. N. Kumar¹, R. Bachiller² and J. M. C. Grave¹

¹ Centro de Astrofísica da Universidade do Porto, Rua das Estrelas, 4150-762 Porto, Portugal

² Observatorio Astronómico Nacional (IGN), Calle Alfonso XII, 3. 28014 Madrid, Spain
e-mail: nanda@astro.up.pt

November 6, 2018

ABSTRACT

Aims. To map the jets and outflows from the Serpens South star forming region and find an empirical relationship between the magnetic field and outflow orientation.

Methods. Near-infrared H₂ $v=1-0$ S(1) 2.122 μ m -line imaging of the $\sim 30'$ -long filamentary shaped Serpens South star forming region was carried out. K_s broadband imaging of the same region was used for continuum subtraction. Candidate driving sources of the mapped jets/outflows are identified from the list of known protostars and young stars in this region, which was derived from studies using recent *Spitzer* and *Herschel* telescope observations.

Results. 14 Molecular Hydrogen emission-line objects (MHOs) are identified using our continuum-subtracted images. They are found to constitute ten individual flows. Out of these, nine flows are located in the lower-half (southern) part of the Serpens South filament, and one flow is located at the northern tip of the filament. Four flows are driven by well-identified Class 0 protostars, while the remaining six flows are driven by candidate protostars mostly in the Class I stage, based on the *Spitzer* and *Herschel* observations. The orientation of the outflows is systematically perpendicular to the direction of the near-infrared polarization vector, recently published in the literature. No significant correlation was observed between the orientation of the flows and the axis of the filamentary cloud.

Key words. Stars: formation - open clusters and associations: individual (Serpens South) - infrared: stars - ISM: clouds - ISM: jets and outflows

1. Introduction

Star formation is thought to occur in molecular clouds, which are largely known to have a filamentary structure owing primarily to the dominant role of turbulence inside them (Nakamura et al. 2011). Our understanding of the details of star formation is largely benefited by observational studies of clean templates of nearby filamentary molecular clouds. A recently discovered filamentary cloud and its associated protocluster (Gutermuth et al. 2008) in Serpens South can be used as one such template.

The Serpens South protocluster is located in the center of a well-defined filamentary cloud that appears as a dark patch in the *Spitzer* 8 μ m image with an approximate extent of 30' in length, and is thought to be part of the larger Serpens-Aquila rift molecular cloud complex (Bontemps et al. 2010; Gutermuth et al. 2008; André et al. 2010). The short distance to this region of ~ 260 pc (Gutermuth et al. 2008; Bontemps et al. 2010) places it among one of the nearest star-forming regions, making it an interesting target in the studies of star formation.

A swath of new infrared and submillimeter observations has been recently used to study various aspects of this star-forming cloud. Gutermuth et al. (2008) used *Spitzer*-IRAC observations to uncover the embedded young star population. Bontemps et al. (2010) presented submillimeter observations performed with *Herschel* Space telescope and identified several Class 0 protostars and candidate protostars in, and around, the filament. Sugitani et al. (2011) mapped the magnetic field associated with this filamentary cloud using near-infrared po-

larimetric observations. Molecular outflows in this region were traced by Nakamura et al. (2011) using CO(J=3-2) observations. Together, these observations, have provided a rich characterization of the Serpens South star-forming region.

The motivation for the study presented in this paper primarily arose from the availability of magnetic field measurements of the entire filament. It is well known, from star formation theories, that the bipolar outflows in young stars are ejected in the direction of the polar axis, to which the magnetic field is also aligned (Tamura et al. 1989). In particular, there is some indication that the outflow activity is orthogonally aligned with the axis of a filamentary cloud (Anathpindika & Whitworth 2008), owing to the nature of the formation of prestellar cores due to the inflows along the filament (Banarjee et al. 2006). It is possible that the presence of an ordered magnetic field on the global scale of the filament may be related to an improved coherence of the orientation of the outflows with respect to the cloud axis. For example, in the DR21/W75 region, a statistically significant coherence was found in the direction of the flows (Davis et al. 2007; Kumar et al. 2007). The magnetic field measurements of this region presented by Kirby (2009) agreed quite well with the previous result in terms of alignment between the magnetic field and the cloud axis. However, similar outflow studies in the Orion A cloud did not show any significant correlation of the orientation of the outflows with the filamentary axis (Davis et al. 2009). This lack of consistent results between these two different regions doesn't allow us to settle the issue of a possible relation between the orientation of these two components of star formation.

Send offprint requests to: M. S. N. Kumar; email:nanda@astro.up.pt

arXiv:1204.4946v1 [astro-ph.SR] 22 Apr 2012

Although many outflow components were found for the Serpens South filament by Nakamura et al. (2011), the lower spatial resolution of the radio observations, and the high density of young stars in the protocluster makes it difficult to disentangle and relate the outflow activity with the protostars clearly. Here, we present deep H₂ narrow-band imaging study of the entire Serpens south filament to a) identify the individual components of the flows, by building upon the results of Nakamura et al. (2011), b) associate the flows with the best candidate driving source, and, c) compare the orientations of the flows with that of the global magnetic field measured by Sugitani et al. (2011) and also the axis of the filamentary cloud.

2. Observations

Near-infrared observations were carried out on the nights of 14-17th July 2011 using the 3.5m telescope at the German-Hispanic Astronomical Center at Calar Alto (CAHA). Two pointings were made in order to cover the full filament (Gutermuth et al. 2008). A near-infrared wide-field camera, Omega2000, with a 15.3' field of view and a plate scale of 0.45'' per pixel was used.

Observations in the H₂ $\nu=1-0$ S(1) 2.122 μ m narrow-band filter were made, a nine-point jitter sequence was applied and repeated eight times at each pointing. An exposure time of 60 sec per jitter was fixed, resulting in an integration time of \sim 72 mins. To facilitate continuum subtraction, observations in the K_s broadband filter were obtained using a twenty-point jitter pattern, rerun one additional time at each pointing, with an exposure time of 5 sec, so the final integration time was \sim 4 mins.

Each set of jittered images were median combined to obtain a sky-frame that was then subtracted from each individual image. Alignment of each image was performed using CCDPACK routines in the Starlink¹ suite of software. The final mosaics were achieved using KAPPA and CCDPACK routines in the Starlink.

The K_s broadband images were psf matched and flux scaled to perform continuum subtraction from the H₂ images.

3. Results

The continuum-subtracted H₂ images from our observations cover almost the entire Serpens south filament (roughly 30' in length). However, only two sub-regions display all the detected H₂ emission. Figure. 1 shows the southern part of the filament where most of the H₂ emission is detected. The northern part of the filament is less active, the region with detected emission is shown in Figure. 2.

In these figures, the detected H₂ features are labeled by Molecular Hydrogen emission-line Object (MHO) names following the catalogue system described by Davis et al. (2010). When MHOs are associated with clear bipolar outflows, we use the same catalogue number for both lobes, but we add the suffix 'b' or 'r' if it is, respectively, the blue-shifted or red-shifted lobe.

In naming the MHO features, we first identified all possible bipolar flows and their driving sources as explained below. We started by identifying the presence of bowshock-like features. Then we extended a line tracing the middle of the bowshock until we reached a possible outflow counterpart. When this counterpart exists, the driving source of the MHO should be along the traced line. The driving sources were assumed to be any of the previously identified Class 0 objects (Bontemps et al. 2010) or Class I objects (Gutermuth et al. 2008). In almost all cases a suitable driving source was found. When a bipolar outflow is

identified, the MHO lobe further away in the plane of the sky from the source is assumed to be the blue-shifted lobe while the one closer to the source is assumed to be the red-shifted lobe.

After the well-defined bipolar flows were identified, the remaining MHO features were associated with the most likely driving source, with the aid of *Spitzer* data and the CO maps published by Nakamura et al. (2011). In Figure. 1, all identified flows are marked by solid lines. Diamond symbols represent Class 0 protostars and open circles show Class I young stars. Figure. 5 is a colour composite made using the *Spitzer* MIPS 24 μ m image as red, IRAC 8.0 μ m image as green and H₂ image as blue. This figure covers exactly the same region displayed in Figure. 1 and reveals the dark filament. The CO flows discovered by Nakamura et al. (2011) are also overlaid on this figure which demonstrates how well the identified H₂ flows correspond to the CO emission.

A total of ten flows are identified in the entire Serpens South filament (Figs.1 & 2), out of which five are clearly identified as bipolar. In the remaining, we detected H₂ emission only from one of the lobes. Two well-defined jet-like features and one bipolar nebula delineated by a dark lane (indicating a disk) are also identified. These interesting features are shown in Figure. 3.

In the following we first discuss in detail each flow explaining their morphology and the nature of the identified driving sources. Table. 1 lists the coordinates and morphology of the MHOs. In Table. 2 we list the driving sources, their evolutionary class, and their visibility in various infrared and millimeter bands.

3.1. Catalogued MHOs

MHO 2214b, MHO2214r: MHO2214 is a well-defined bipolar outflow (Figure. 2), with collimated components. Its blueshifted component had been previously discovered by Connelley et al. (2007) but our observations were able to reveal its redshifted counterpart. This enabled us to discover its bipolar nature. The central knot of the blue-shifted component is a distinct bowshock. The source P1, identified as the driving source, is classified as a protostar by Bontemps et al. (2010), and is located equidistantly from both MHO features.

MHO 3247: This MHO feature is represented in Figure. 1 by a dashed arrow, indicating its probable direction. It is a jet-like feature originating from the source P2, classified as a Class 0 protostar by Bontemps et al. (2010) and located in the midst of the protocluster discovered by Gutermuth et al. (2008). No discernable MHO counterpart is found for this feature. Note that this region is the central part of the filament, associated with the dense cluster of young stars and intense, multiple outflow activity (Nakamura et al. 2011) causing much confusion.

MHO 3248: This is a bright MHO feature with a relatively wide opening angle. When compared with the CO maps by Nakamura et al. (2011), it shows clear indications of extending to the south by \sim 317 arcseconds touching the bowshock feature identified as MHO3251b. The most likely driving source of this MHO feature is the Class 0 object marked as P3 in Figure. 1, and is located in the middle of the Serpens South protocluster. This MHO feature appears to be associated with the blue lobes MHO3249b and MHO3251b, outflows with which it has, likely, physically interacted.

MHO 3249b, MHO3249r: These MHO features are identified to delineate a bipolar flow driven by the Class I young star P4 (Bontemps et al. 2010) that appears as an infrared point

¹ <http://starlink.jach.hawaii.edu>

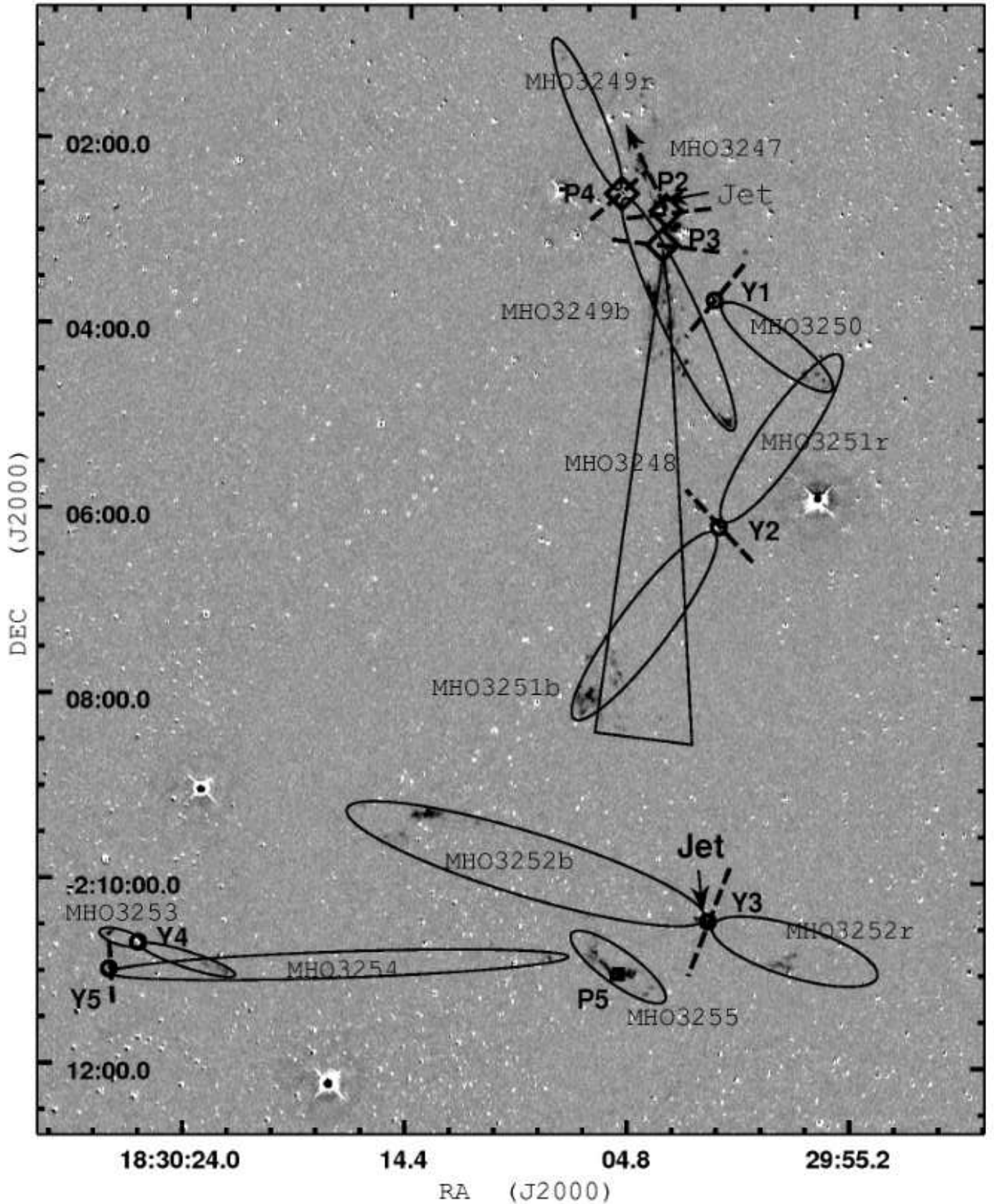


Fig. 1. Continuum-subtracted H_2 image of the southern part of the observed region, displayed with logarithmic scales. The sources are marked according to the following: diamonds represent Class 0 stars from Bontemps et al. (2010), circles are Class I from Bontemps et al. (2010) and the square is a candidate Class 0 observed only in *Spitzer* $24\ \mu\text{m}$, the labels P2, P3, P4, P5, Y1, Y2, Y3, Y4 and Y5 are the names we used to refer to each source throughout our work. For more on the outflows and driving sources see Table. 1. Also visible are dashed lines representing the polarization vectors (Sugitani et al. 2011).

Table 1. List of MHOs and their sources

MHO	Ra	Dec	Size	Source	Comments
MHO2214b	18:29:39.8	-01:51:28	49.5''	P1	Bipolar, bowshock
MHO2214r	18:29:36.0	-01:50:40	40.0''	P1	Bipolar
MHO3247	18:30:04.5	-02:02:17	45.5''	P2	Single lobe, jet-like
MHO3248	18:30:03.4	-02:03:48	317.1''	P3	Single lobe, fan-shaped
MHO3249b	18:30:00.6	-02:05:02	104.5''	P4	Bipolar, clear bowshock
MHO3249r	18:30:07.8	-02:01:06	169.5''	P4	Bipolar, faint arc
MHO3250	18:29:56.2	-02:04:37	92.3''	Y1	Single lobe, bowshock
MHO3251b	18:30:06.8	-02:08:10	152.3''	Y2	Bipolar, bowshock
MHO3251r	18:29:56.8	-02:04:33	129.5''	Y2	Bipolar, faint arc
MHO3252b	18:30:13.5	-02:09:15	237.9''	Y3	Bipolar, clear bowshock, jet
MHO3252r	18:29:58.1	-02:10:56	62.9''	Y3	Bipolar, faint bowshock
MHO3253	18:30:25.8	-02:10:43	25.3''	Y4	Single lobe, bowshock
MHO3254	18:30:22.1	-02:10:59	284.1''	Y4 or Y5	Single, confusion
MHO3255	18:30:05.3	-02:11:00	52.4''	P5	Bipolar, embedded source

source and is associated with significant millimeter continuum emission. The southern, blue lobe ends in a clear, sharply defined bowshock. The red-shifted component has a single, poorly-defined knot but the fact that it is well-aligned with the source and the blue-shifted lobe allows us to determine that they are part of the same bipolar flow. MHO3249b shows indications of crossing and/or being physically in contact with the outflow lobe associated with MHO3248. Nevertheless, the well-defined bowshock associated with this lobe unambiguously identifies the outflow lobe and the driving source.

MHO 3250: MHO3250 is composed of two visible H₂ knots and delineates one of the lobes of an outflow driven by the Class I young star marked as Y1. There is indication that this poorly defined MHO crosses paths with another nearby flow associated with MHO3251r.

MHO 3251b, MHO3251r: These MHO features are associated with a well-identified bipolar outflow, originating in the Class I young star Y2 (Bontemps et al. 2010). The red and blue lobes are nearly equidistant from the source (see Figure. 1) suggesting that this flow is in the plane of the sky. This fact is further supported by the detection of a clear, bipolar-shaped nebula visible in the K_s band images. The bipolar nebula is divided by a dark strip showing a clear sign of the presence of an edge-on disk in the source. This edge-on disk is zoomed and displayed in Figure. 3a. The MHO features align perpendicular to the disk feature, the blue lobe MHO3251b terminates in a well-defined bowshock and MHO3251r is composed of two knots. The presence of another MHO, MHO3250, near the red-shifted component is the source of some confusion but not as to significantly change our conclusions.

MHO 3252b, MHO3252r: These MHO features are away to the south of the confusing central protocluster. MHO3252b consists of a clear H₂ jet originating from the Class I young star marked as Y3 (Bontemps et al. 2010). The YSO is visible even in the near-infrared K_s band and is also associated with a clear millimeter core identified from *Herschel* observations. The blue lobe driven by this source, terminates in a distinct arc-like H₂ feature, while the red-shifted lobe is traced by a group of H₂ knots. This flow is bright enough to be visible prominently even in the color composite image (see Figure. 5).

Table 2. List of driving sources

Source	Ra	Dec	Source Type	Wavelengths(μm)
P1	18:29:38.0	-01:51:01	Class 0	24
P2	18:30:03.2	-02:02:45	Class 0	8-24
P3	18:30:03.6	-02:03:11	Class 0	24
P4	18:30:05.2	-02:02:34	Class I	3.6-24
Y1	18:30:01.2	-02:03:43	Class I	2.15-24
Y2	18:30:00.9	-02:06:10	Class I	2.15-24
Y3	18:30:01.3	-02:10:26	Class I	2.15-24
Y4	18:30:25.8	-02:10:43	Class I	2.15-24
Y5	18:30:27.2	-02:11:00	Class I	2.15-24
P5	18:30:05.3	-02:11:00		24

MHO 3253: MHO3253 could be classified as a bipolar outflow but since part of the outflow crosses MHO3254 we only address the northern lobe, a clear arc-like structure originating in the nearby Class I source, Y4 (Bontemps et al. 2010).

MHO 3254: This feature is probably associated with a flow driven by a Class I YSO, marked as Y5 in Fig. 1. The eastern part of this outflow shows a single knot in the direction of the source which overlaps with the possible bipolar flow originating from MHO3253, causing some confusion.

MHO 3255: This H₂ feature has the morphology of a wiggly bowshock. At the outset, it is likely the tip of a very long flow originating from the Class 0 source P3, that is situated at the center of the protocluster. A careful analysis of *Spitzer* MIPS-24μm images, nevertheless, reveals a faint source marked P5 in Figure. 1, located in the middle of this H₂ emission. Furthermore, this faint MIPS source is also associated with weak millimeter continuum emission identified by *Herschel* observations as candidate protostar. Therefore, we suggest that MHO3255 is a weak outflow with a very young age driven by the candidate protostar P5. The wiggly bow-shape of the H₂ features may then be due to the motion of this source in the plane of the sky.

Finally, we examined the *Spitzer* 4.5μm images analyzed by Gutermuth et al. (2008) to uncover any hidden census of outflows that might have escaped detection in our near-infrared data. The *Spitzer*-IRAC 4.5μm band is known to encompass a bright H₂ emission line, and, the extinction at this wavelength

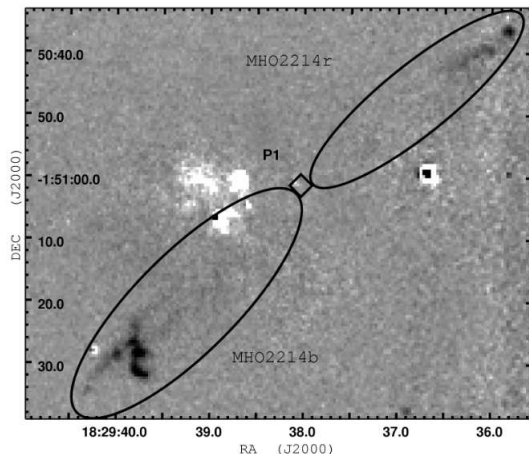


Fig. 2. Continuum-subtracted H_2 image of the northern part of the observed region, displayed with logarithmic scales. This bipolar outflow well aligned with Class 0 protostar P1 (Bontemps et al. 2010).

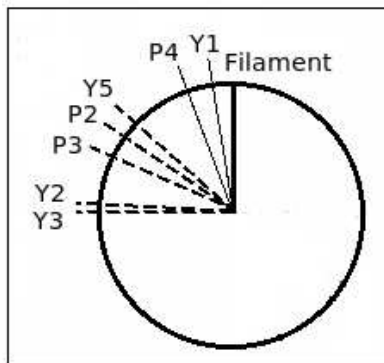


Fig. 4. Positional angles (PA) of the sources polarization relative to the PA of the filament (0 degrees). Solid and dashed lines show $PA < 45^\circ$ and $PA > 45^\circ$ respectively.

is roughly half as much as in the K band (Flaherty et al. 2007). Although almost all of our detected outflows are also present on those images there is no visible indication for the existence of additional outflows in the studied area. Indeed, the H_2 data presented here provide the certainty of tracing pure emission line features unlike the $4.5\mu\text{m}$ data where judgement is based on comparison with other bands and not real continuum subtraction. Further, our H_2 data offers a superior spatial resolution disentangling the morphological details. Not detecting additional features from *Spitzer* data is an indication that the outflow sample traced by our data is quite complete and the extinction in this cloud is similar to other nearby regions of star formation where H_2 narrow-band images effectively serve as jet/outflow tracers.

4. Discussion

In the studied region we found a total of ten outflows, five of which are clearly bipolar and only a single lobe was detected in the remaining five MHOs. We then studied the collimation factors of each MHO, defined as the ratio between the length and the width of each outflow. At least two of the observed

MHOs have high collimation factors, particularly MHO3249r and MHO3254, with collimation factors of 11.2 and 15.6 respectively. These examples of extreme collimation can be directly linked to the young nature of these sources and may be an indication of the presence of high velocity components (Bachiller 1996). On the other hand, we also observe some outflows that present low collimation factors (between 2 and 5), MHO3253, MHO3252r and MHO2214b with factors of 2.5, 4.2 and 4.6 respectively. These low collimation factors point towards the fact that the origin of these outflows lies in ambient gas picked up by stellar winds (Bachiller 1996).

We also performed a rough comparison between the orientation of the MHOs and the axis of the cloud filament. Outflows were considered parallel to the filament if their orientation angle with respect to the axis of the filament is less than 45° and perpendicular when the angle was greater than 45° . This comparison showed that $\sim 71\%$ of the flows are perpendicular and $\sim 29\%$ are parallel to the filament. In Figure 4 we plotted the positional angles (PA) of the known polarization vectors relative to the PA of the filament or subfilament where each source is located, in order to observe the distribution of parallel and perpendicular vectors. Although these fractions are similar to the values obtained by Anathpindika & Whitworth (2008) ($\sim 72\%$ perpendicular and $\sim 28\%$ parallel), we stress that our sample is not large enough to be statistically significant. Although we cannot imply the existence of a coherent pattern in the orientation of the outflows due to poor statistics, our analysis demonstrates that the fraction of flows perpendicular to the filament are clearly larger than those parallel to the filament.

Nevertheless, we find a better correlation between the orientation of the outflows with respect to the local magnetic field. To obtain this result, we compared the direction of MHO flows with that of the near-infrared polarization vectors of the driving sources (obtained from the data of Sugitani et al. 2011). We were able to find polarization vectors associated with seven identified driving sources, namely P2, P3, P4, Y1, Y2, Y3 and Y5. These vectors are shown as dashed lines in Figure 1. In all these cases, the outflows are generally found to be perpendicular to the polarization vectors. In particular, the polarization vector of source Y2, traces perfectly the disk of that young star (see Figure 3) which is identified as a dark lane cutting across a bipolar reflection nebula, and is found to be perpendicular to MHO3251.

Polarization measurements of light from young stars are known to represent the disks and envelopes rather than the embedded proto-star. This is because, the light originating in the young star is reprocessed in the dense envelopes surrounding them before reaching the observer. Therefore, the observed polarization vectors are usually found to be parallel to the disk axis which is perpendicular to the axis of the stellar magnetic field (Tamura et al. 1989; Pereyra et al. 2009; Murakawa 2010). In fact, the level of polarization is found to increase in younger sources and/or edge-on disks (Greaves et al. 1997).

It is known that outflows follow the open magnetic lines of the source, which means that their origin should be near the magnetic poles of the source (Königl et al. 2011). Since the majority of the observed outflows are perpendicular to the known polarization vectors we can conclude that the observed polarization vectors are perpendicular to the magnetic field of the driving sources. Given this close relation between the local magnetic field and the arrangement of MHOs, it is clear that the outflows are aligned with the local magnetic field. While the large scale orientation of the polarization vectors roughly run perpendicular to the axis of the filamentary cloud, local twists are found to exist from the observations of Sugitani et al. (2011). The location

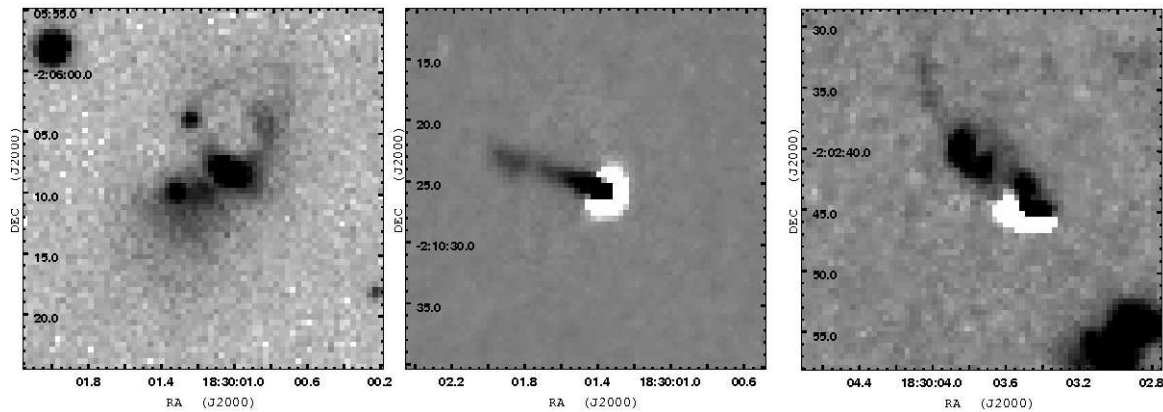


Fig. 3. From left to right the images are centered on: the bipolar nebula of Y2 visible in the K_s broadband filter, the outflow jet from Y3, on a continuum-subtracted image, and the the jet from P2, also in a continuum-subtracted image.

of the driving sources along such twists may, therefore, indicate the position of star forming cores. As accretion proceeds, the magnetic field appears to become distorted, so we don't expect or observe any coherent alignment between the global magnetic field and the orientation of the MHOs (Pereyra et al. 2009). This is likely one of the reasons we do not find a high degree of coherence between the orientation of the flows with the filamentary axis. Other factors such as turbulence, the morphology of the filament at smaller scales and the distribution of cores can also strongly influence the deviations of the local magnetic fields from the global field.

5. Summary and Conclusions

We discovered new MHO features in the filamentary molecular cloud "Serpens South" associated with a protocluster, in the Aquila Rift. We have catalogued MHO features associated with 10 outflows, five of which are clearly identified as bipolar outflows (Table. 1). A comparison between our survey and previous images obtained with *Spitzer* showed no additional MHOs in the region. Two jet-like features, launched from the driving YSOs are clearly identified. One edge-on disk in this region is also identified from this study (see the bipolar nebula in Figure. 3). Half of the detected flows are identified to be driven by previously classified Class 0 objects and the remaining half are driven by Class I type sources. The MHO features found here are well associated with the CO outflows presented by Nakamura et al. (2011). In particular, MHO3247, MHO3248, MHO3251 and MHO3252 appear to trace the CO maps extremely well matching the blue or red shifted lobes.

We find that two of the observed MHOs have high collimation factors, indicating that we are dealing with high velocity flows.

Our H_2 imaging study has allowed disentangling and clarifying the association between outflows and driving sources in the central protocluster. The high concentration of outflows from the protocluster located at the center of the filamentary cloud displayed some confusion that did not permit an unambiguous association of the outflows and their sources. Our results also indicate that the flows launched from the central protocluster may have interacted with each other physically since they are launched from a small region. MHO3248 and MHO3249b are two such signatures.

We show that the near-infrared polarization vectors mapped by Sugitani et al. (2011) are perpendicular to the outflows and

therefore to the magnetic field of the sources. While the outflows are perpendicular to the local polarization vectors, no specific coherence is found with respect to the global pattern. Despite dealing with a sample that is statistically not significant, we find that $\sim 71\%$ of the flows in this region are perpendicular to the axis of the filamentary cloud, see Fig. 4, an estimate that agrees well with the previous work by Anathpindika & Whitworth (2008).

Acknowledgements. We thank F. Nakamura for providing the CO data for overplotting in the colour Figure. Teixeira acknowledges support from a Marie-Curie IRSES grant (230843) under the auspices of which, part of this work was carried out. Kumar is supported by a Ciéncia 2007 contract, funded by FCT/MCTES (Portugal) and POPH/FSE (EC). We also thank the staff at the Calar Alto observatory for their support.

References

- Anathpindika, S., Whitworth, A. P. 2008, A&A, 487, 605
- André, P., et al., 2010, A&A, 518, L102
- Bachiller, R. 1996, ARA&A, 34, 111
- Banarjee, R., Pudritz, R. 2006, ApJ, 641, 949
- Bontemps, S., André, P., Könyves, V., et al. 2010, A&A, 518, L85
- Connelley, Michael S., Reipurth, Bo, Tokunaga, Alan T., 2007, AJ, 133, 1528
- Davis, C. J., Kumar, M. S. N., Sandell, G., Froebrich, D., Smith, M. D., Currie, 2007 MNRAS, 374, 29
- Davis, C. J., Froebrich, D., Stanke, T., Megeath, S. T., Kumar, M. S. N. et al. 2009, A&A, 496, 153
- Davis, C. J., Gell, R., Khanzadyan, T., Smith, M. D., & Jenness, T., 2010, A&A, 511, A24
- Flaherty, K. M., Pipher, J. L., Megeath, S. T., Winston, E. M., Gutermuth, R. A., Muzerolle, J., Allen, L. E. & Fazio, G. G. 2007, ApJ, 663, 1069
- Gorvola, N., Steinhauer, A., Lada, E. 2010, ApJ, 716, 634
- Greaves, J. S., Holland, W. S., Ward-Thompson, D. 1997, ApJ, 480, 255
- Gutermuth, R. A., Bourke, T. L., Allen, L. E., et al. 2008, ApJ, 673, L151
- Kirby, L., 2009, ApJ, 694, 1056
- Königl, A., Romanova, M., Lovelace, R. 2011, MNRAS, 416, 757
- Kumar, M. S. N., Davis, C. J., Grave, J., Ferreira, B., Froebrich, D., 2007 MNRAS, 374, 54
- Lada, C., Lada, E. 2003 ARA&A, 41, 57
- Murakawa, K. 2010, A&A, 518, 63
- Nakamura, F., Sugitani, K., Shimajiri, Y., et al. 2011, ApJ, 737, 56
- Pereyra, A., Girart, J., et al. 2009, A&A, 501, 595
- Sugitani, K., Nakamura, F., Watanabe, M., et al. 2011, ApJ, 734, 63
- Tamura, M., Sato, S. 1989, AJ, 98, 1368

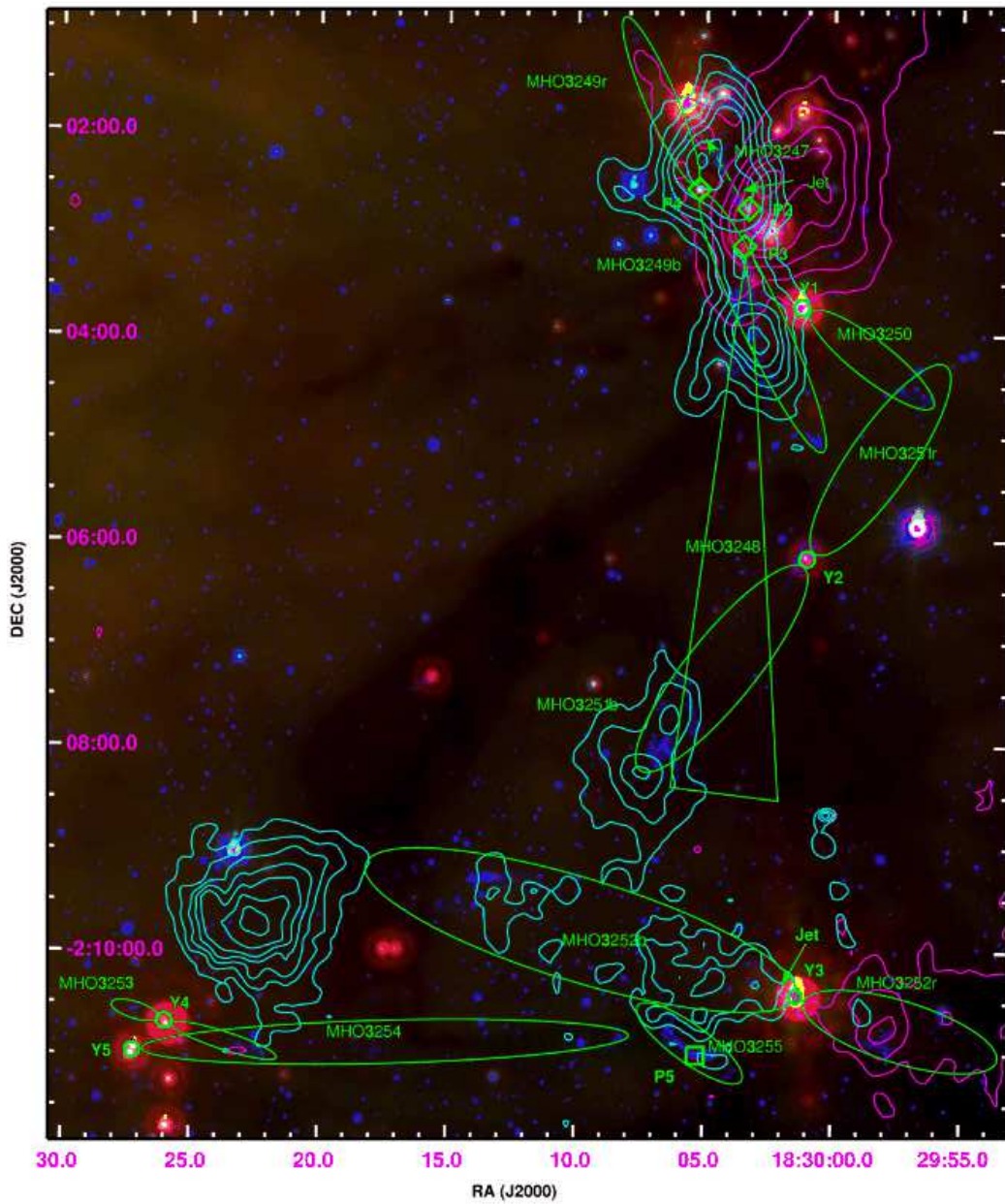


Fig. 5. A colour image of the southern region studied. *Spitzer* MIPS $24\mu\text{m}$ is red, *Spitzer* MIPS $4.5\mu\text{m}$ is green and H_2 narrowband image as blue. The images use a logarithmic scale. The red and blue shifted CO emission mapped by Nakamura et al. (2011) is displayed using, respectively, pink and blue contours.